CHAPTER 2

CHARACTERIZATION OF THE REC TECHNIQUE

2.1 The Effects of Nonlinear Distortion on the Compression of REC Echoes

2.1.1 Introduction

In ultrasound, when the excitation waveform is low in pressure amplitude, wave propagation is described by the linear wave equation. In the development of the linear wave equation, the higher order terms in the general acoustic equations (equation of state, equation of continuity, Euler's equation of force) are negligible. The one-dimensional linear wave equation [20] is

$$\frac{\partial^2 \xi}{\partial t^2} = c_0 \frac{\partial^2 \xi}{\partial x^2} \tag{2.1}$$

where c_0 is the small signal speed of sound, ξ is the particle displacement, and t is time.

In cases where low pressure amplitudes are used, the eSNR may be relatively low, which in turn provides poor sensitivity. Therefore, larger pressure amplitudes may be necessary to improve the eSNR but at the expense of possible nonlinear effects of the medium that distort the pressure wave. To further understand the effects of nonlinearity, the development of the linear wave equation must be modified to include higher order terms.

In the derivation of the linear wave equation the higher order terms from the Taylor series expansion of the equation of state were assumed to be negligible. For the nonlinear equation of state the quadratic and linear terms of the Taylor series are used. Specifically, the nonlinear equation of state [21] is expressed as

$$p = As + \frac{B}{2}s^2, \tag{2.2}$$

where s is the condensation. Furthermore, A and B are defined as:

$$A = \rho_0(\frac{\partial P}{\partial \rho}) = \rho_0 c_0^2 \tag{2.3}$$

$$B = \rho_0^2(\frac{\partial^2 P}{\partial \rho^2}), \tag{2.4}$$

where ρ_0 is the ambient density, ρ is density, and P is the total pressure. Moreover, the one-dimensional nonlinear continuity equation [21] can be described by

$$s = -\frac{\partial \xi}{\partial x}(1 - \frac{\partial \xi}{\partial x}), \tag{2.5}$$

where x is the spatial coordinate. If expression (2.5) was substituted into (2.2) and then only the linear and quadratic terms were kept, the resulting development can be obtained:

$$p = -A\frac{\partial \xi}{\partial x} + A\beta_n(\frac{\partial \xi}{\partial x})^2, \tag{2.6}$$

where β_n [22] is a parameter that quantifies the nonlinear properties of the medium and is referred to as the Beyer parameter or the coefficient of nonlinearity. The Beyer [22] parameter is given by

$$\beta_n = 1 + \frac{B}{2A}, \tag{2.7}$$

where the ratio B/A [20] is

$$B/A = \frac{\rho_0}{c_0^2}(\frac{\partial^2 P}{\partial \rho^2}). \tag{2.8}$$

The expression in (2.6) can be substituted into the 1D Euler's equation [20] which yields

$$-\nabla_x p = -\frac{\partial p}{\partial x}. \tag{2.9}$$

The resulting expression is the nonlinear wave equation:

$$\frac{\partial^2 \xi}{\partial t^2} = c\frac{\partial^2 \xi}{\partial x^2}, \tag{2.10}$$

where c is defined as

$$c = c_0[1 - 2\beta_n(\frac{\partial \xi}{\partial x})]. \tag{2.11}$$

A comparison between the linear and nonlinear wave equations suggests that any vari-

ation in the pressure is a result of changes in the speed of sound. In fact, the speed of sound term can be approximately written as [21]

$$c = c_0 + \beta_n u \tag{2.12}$$

where u is the particle velocity. For a linear system, β is zero and the nonlinear wave equation reverts to the classical wave equation. In the nonlinear case, the speed of sound will be a function of the small signal speed of sound and particle velocity. For a plane wave, pressure is proportional to particle velocity. Therefore, the nonlinear effects arise from the fact that the speed of the wave is a function of pressure. The compressional portion of the pressure wave travels faster than the rarefactional portion, which causes the overall waveform to distort as shown in Fig. 2.1. This distortion comes from the transfer of energy from the fundamental into higher harmonics. Besides nonlinear propagation resulting from the medium characteristics, odd harmonics can be generated by the crystal geometry of the transducer.

In terms of coded excitation and pulse compression, it was hypothesized that nonlinear distortion could be detrimental to the compression performance when using a Wiener filter with a smoothing parameter. If the operating point of the Wiener filter were to approach an inverse filter, then the harmonics could be significantly amplified causing a large mismatch between the excitation signal and the received signal. Nonetheless, several researchers have taken advantage of the nonlinear distortion to improve the contrast-to-tissue ratio (CTR) when using coded excitation. Borsboom et al. [23, 24] found that with a chirped excitation the response of a microbubble was 3 and 6 dB higher for the second and third harmonics, respectively, when compared to conventional pulsing techniques. In that work, compression was performed by using a matched filter based on the harmonic components resulting in a sidelobe-to-mainlobe ratio of -60 dB. Chiao and Xiaohui [3] evaluated simulations of nonlinear distortion using phase codes to quantify the tradeoff of penetration depth and resolution by using a matched filter. However, the effects that nonlinear distortion may have on the compression of coded signals when using a Wiener filter have not been fully evaluated, specifically in an experimental setting.

2.1.2 Methods and procedures

In this study, the effects of nonlinear distortion on the compression of coded excitation echoes when using a Wiener filter were evaluated. Typically, when nonlinear distortion is not present, operating the Wiener filter as an inverse filter reduces the sidelobe levels and provides the best performance in terms of axial resolution. However, an inverse filter has the side effect of boosting the noise outside of the transducer's passband. When nonlinear distortion is present, using a Wiener filter that closely approximates an inverse filter will result in amplification of the harmonics in the signal. The amplification of the harmonics from the filter could result in a loss of the axial resolution enhancement and increased sidelobe levels. One possible solution to this problem would be to prefilter the echo signals to remove the higher harmonics before applying the compression filter.

Image quality metrics

To evaluate the effects that nonlinear distortion may have on the compression of coded excitation echoes, the following image quality metrics were used:

1. Compressional-to-rarefactional pressure amplitude ratio (CRPR): CRPR is used to quantify the asymmetry in the amplitude of the pressure wave as result of nonlinear distortion [25]. CRPR was evaluated pre- and post-compression.

2. Second-harmonic-to-fundamental ratio (SHFR): SHFR is the ratio of the amplitude of the center frequency of the second harmonic to the amplitude of the center frequency of the fundamental [25]. The higher the SHFR, the more significant the nonlinear distortion will become. SHFR was evaluated pre- and post-compression.

3. Sidelobe-to-mainlobe ratio (SMR): SMR is an important metric used to determine the quality of the compression and is defined by quantifying sptial sidelobes using

$$SMR(x) = 20 \cdot \log_{10}\left(\frac{g^{'}_{sidelobe}(x)}{g^{'}_{mainlobe}(x)}\right), \tag{2.13}$$

   where $g^{'}(x)$ is the echo waveform. There is no gold standard in terms of acceptable sidelobe levels; however, [15] suggests that -45 dB is acceptable for most ultrasonic imaging purposes. For this work, short range sidelobes will be defined as those

sidelobes within one mainlobe width from the mainlobe while long range sidelobes are defined as all other sidelobes.

4. Modulation transfer function (MTF): MTF [26] is an important metric for determining axial resolution of an imaging system. MTF is the magnitude of the optical transfer function and is defined by

$$MTF(k) = \left|\frac{H(k)}{H(0)}\right|, \tag{2.14}$$

where $H(k)$ is the spatial Fourier transform of the envelope of the compressed waveform. The wave number value, k_0, where the value of the MTF curve is 0.1, is used to determine the axial resolution of the imaging system. The axial resolution is defined as

$$\lambda = 1/2 \cdot (2\pi)/k_0. \tag{2.15}$$

Experimental setup

To evaluate the effects of nonlinear distortion, experimental measurements were acquired in pulse-echo mode with a single-element (f/3) transducer (Panametrics, Waltham, MA) having a center frequency of 5 MHz and a -6 dB bandwidth of 74%. The bandwidth was increased to 148% using REC. The experimental setup consisted of generating a pre-enhanced chirp in MATLAB (The Mathworks Inc., Natick, MA). The resulting waveform was then downloaded to an arbitrary waveform generator (Tabor Electronics W1281A, Tel Hanan, Israel). The excitation signal was sampled at a rate of 100 MHz and amplified by an RF power amplifier (ENI 3251, Rochester, NY). The amplified signal (50 dB) was connected to the transducer through a diplexer (Ritec RDX-6, Warwick, RI). The echo signal was received by a pulser-receiver (Panametrics 5800, Waltham, MA), which was displayed on an oscilloscope (Lecroy 9354 TM, Chester Ridge, NY) for visual verification. The echo signal was recorded at a rate of 100 MHz by a 12-bit A/D (Strategic Test Digitizing Board UF3025, Cambridge, MA) for further processing by a PC. In addition to pulse-echo measurements, a Marconi hydrophone was used to obtain pressure measurements at the focus of the source. When in pulse-echo mode, the target used for imaging was a Plexiglas reflector located at the focus of the source.

To quantify the effects of nonlinear distortion on the compression, the pre-enhanced chirp was evaluated at four different output excitation voltage levels from the Tabor arbitrary waveform generator: 18 mV, 178 mV, 355 mV, and 710 mV. These voltages, which correspond the the peak amplitude in the pre-enhanced chirp, were amplified by 50 dB with a power amplifier. The pressure waves at the focus of the transducer were acquired with a calibrated hydrophone. The respective rarefactional pressure levels were estimated at: 69.7 kPa, 1.3 MPa, 2.7 MPa, and 4.0 MPa, respectively.

To predict the nonlinear distortion of the waveforms based on the pressure values, the discontinuity distance was calculated. The discontinuity distance is defined as the distance where significant nonlinear distortions of the waveform occur. The discontinuity distance, L_d, [20] is given by:

$$L_d = \frac{1}{\beta M k}. \tag{2.16}$$

B/A is equal to 5 for water at 20 °C. M [20] is the mach number which is defined as

$$M = \frac{U_0}{c_o} = \frac{P_0}{\rho c_o^2}, \tag{2.17}$$

where U_0 and P_0 are the particle velocity and pressure of the wave, and ρ and c_0 are the density and the speed of sound of the medium, i.e., water. Finally, k is the acoustic wave number. From (2.16), the pressure needed to produce significant nonlinear distortion of the waveform at a distance of 57 mm with a 5 MHz source proapagating in water is 517 kPa. Hence, at 517 kPa it is expected that significant effects of nonlinear distortion will start to occur.

2.1.3 Results

The pre-compression CRPRs for the aforementioned pressure levels were 1.14, 1.18, 1.16, and 1.23, respectively, suggesting higher waveform assymetry for the higher pressure values used. Similarly, the pre-compression SHFRs were -30.3 dB, -30.7 dB, -31.7 dB, and -24.9 dB, respectively, suggesting more energy was transferred to the higher harmonics with the increased pressure. The results from the first three pressure levels were not very different from each other. Therefore, these results indicated that nonlinear distortion effects were most visible for the 4.0 MPa case. Therefore, to simplify the discussion,

the 1.3 MPa and the 4.0 MPa cases were examined in further detail.

The PSD of REC compressed signals evaluated for three different γ parameters along with the CP reference are shown in Fig. 2.2(a). The three γ parameters were chosen in order to establish the effects of nonlinear distortion on the compression performance when matched filtering, inverse filtering and the operating state in between matched and inverse filtering were used. The SHFRs after compression for the 1.3 MPa and the 4.0 MPa cases as the Wiener filter approached a matched filter were -70 dB and -36 dB, respectively. These results suggest that a matched filter aids in the reduction of the nonlinear effects as the 1.3 MPa case resulted in an approximate decrease of 40 dB in the SHFR while the 4 MPa case saw an approximate reduction of 11 dB in the SHFR. However, a matched filter is known to introduce sidelobes as observed in Fig. 2.2(b). For example, the SMR results have short-range sidelobes at -25 dB and -20 dB and long-range sidelobes at -37 dB and -32 dB for the 1.3 MPa and 4 MPa REC cases, respectively. Another detriment of matched filtering is that the resolution suffers as the signal length increases due to the correlation. As a consequence, the MTF results shown in Fig. 2.2(c) indicate that the axial resolution for CP was 209 μm while the axial resolutions for the 1.3 MPa and 4 MPa cases were 300 μm and 298 μm. Overall, nonlinear distortion did not significantly affect the compression results when using a Wiener filter that approached a matched filter. However, for improving axial resolution and maintaining small sidelobes, the matched filter is not ideal.

On the other extreme, as the Wiener filter approached an inverse filter the opposite effects were encountered. In Fig. 2.2(a) it is clearly visible that the second harmonic and even the third harmonic (for the 4 MPa case) were stronger than the fundamental. As the Wiener filter approached an inverse filter the SHFR after compression for the 1.3 MPa and the 4.0 MPa cases were -0 dB. These results suggest that when nonlinear distortion is present, an inverse filter based on the impulse response of the system is detrimental as the 1.3 MPa case was characterized by an approximate increase of 17 dB in second harmonic amplitude while the 4 MPa case was characterized by an approximate increase of 25 dB in second harmonic amplitude. This increase in harmonic power led to larger sidelobe levels as shown in Fig. 2.2(b), which is especially noticeable when comparing the two pressure levels. For the 4 MPa case, the SMR short-range sidelobes

started at -10 dB while the long-range sidelobes were at -20 dB. For the 1.3 MPa case, the SMR short-range sidelobes started at -14 dB while the long-range sidelobes were at -30 dB. Furthermore, the MTF results revealed that the axial resolution for the 4 MPa case suffered because of the harmonic boost caused by the Wiener filter as it approached an inverse filter. Specifically, the evaluation of the MTF in Fig. 2.2(c) resulted in estimated axial resolution values for the 1.3 MPa and 4 MPa cases of 138 μm and 269 μm, respectively. Overall, nonlinear distortion negatively affected the compression, specifically by increasing the sidelobes and decreasing the axial resolution, when using a Wiener filter that approached an inverse filter.

A middle approach would be to use the gamma parameter to select a point between these the inverse and matched filter. Figure 2.2(a) indicates that for the case where the Wiener filter was between an inverse and matched filter response, the SHFR for the 1.3 MPa and the 4.0 MPa cases were -31 dB and -17 dB, respectively. For the 1.3 MPa case, the SMR was -30 dB for the short-range sidelobes and was -35 dB for the long-range sidelobes. For the 4 MPa case, the SMR was -32 dB for short-range sidelobes and was -34 dB for the long-range sidelobes. The values for the axial resolution determined by the MTF was 166 μm for the 1.3 MPa case and 151 μm for the 4 MPa case. In this approach, improvements in axial resolution were achieved compared to the matched filtering case. Furthermore, sidelobe levels were moderately improved when compared to both matched filtering and inverse filtering. These results along with the results for the matched filtering and inverse filtering case are summarized in Table 2.1

Pre-compression filtering

In the previous analysis, only changes in the gamma parameter were used to address the effects of nonlinear distortion. However, alternate schemes can be used to address nonlinear distortion effects in pulse compression. By applying a band-pass filter prior to compression, the harmonic content introduced by the nonlinear distortion could be suppressed and, as a consequence, improve the performance of the compression. To illustrate, a simple frequency domain Tukey window band-pass filter with a 50% taper ratio was applied to the pre-compressed echo data as shown in Fig. 2.3. The equation describing the Tukey window is as follows:

$$w(n) = \begin{cases} 1.0, & 0 \leq |n| \leq \alpha\frac{N}{2} \\ 1/2(1+\cos(\pi\frac{n-\alpha\frac{N}{2}}{2(1-\alpha)\frac{N}{2}})), & \alpha\frac{N}{2} \leq |n| \leq \frac{N}{2}. \end{cases} \tag{2.18}$$

The PSDs of REC compressed results evaluated for three different gamma parameters along with the CP reference are shown in Fig. 2.4(a). For all three Wiener filter scenarios, the SHFR values after compression for both the 1.3 MPa and the 4.0 MPa cases were well below -50 dB. The matched filter had SMR values of -19 dB for the short-range sidelobes and and -50 dB for the long-range sidelobes in the 1.3 MPa case. For the 4 MPa case, the SMR was -20 dB and -47 dB for the short- and long-range sidelobes, respectively.

In the case of an inverse filter, the sidelobe levels had an SMR of -22 dB for the short-range sidelobes and -45 dB for the long-range sidelobes for both 1.3 MPa and 4 MPa cases. These results suggest that the pre-compression filtering not only improved the compression results by removing the harmonics introduced by nonlinearities as shown in the 4 MPa case, but also aided in the reduction of sidelobe levels when the harmonic content was not as dominating as in the 1.3 MPa case.

MTF analysis resulted in estimates of the axial resolution for CP of 209 μm. The values of the axial resolution determined through the MTF using pre-compression filtering and then an inverse filter were 128 and 127 μm for the 1.3 MPa and 4 MPa cases, respectively. For the matched filter case, the axial resolution values were 148 and 137 μm for the 1.3 MPa and 4 MPa cases, respectively. Based on these results, the pre-compression filtering of the echo signals resulted in significant benefits in terms of reduction in sidelobe levels and improvements in axial resolution.

The effects of attenuation on nonlinear distortion when exciting with a pre-enhanced chirp

In soft tissues, ultrasonic attenuation typically increases with frequency. Consequently, the effects of nonlinear distortion are minimized in some fashion when imaging soft tissues due to the frequency-dependent attenuation. Specifically, the effects of nonlinear distortion are reduced because the higher frequency harmonic content is attenuated more rapidly than the fundamental. As a result, nonlinear distortion result in ex-

cess attenuation of the signal. Values highlighting the attenuation coefficients [27] of several human soft tissues are listed in Table 2.2. To evaluate the effects of frequency-dependent attenuation on the echoes that have been distorted by nonlinear propagation, the uncompressed echo data were modified by multiplying with a frequency-dependent attenuation term to simulate the effects of tissue attenuation synthetically on experimental data. Based on the range of attenuation coefficient values listed in Table 2.2 [28], attenuation coefficients of 0.0, 0.1, 0.3, 0.5, and 1.0 dB $\mathrm{MHz}^{-1}\mathrm{cm}^{-1}$ were evaluated.

The SHFR results for the aforementioned attenuation coefficient values are listed in Table 2.3. Furthermore, in Fig. 2.5 it can be observed from the PSD that the harmonic content was reduced as the attenuation coefficient increased. These results indicate that frequency-dependent attenuation aided the compression by mitigating some of the effects caused by nonlinear distortion of the signal. Even though attenuation appears to be beneficial, i.e., it ameliorated some of the effects brought on by nonlinear propagation, attenuation naturally reduced the bandwidth of the imaging system as shown in Fig. 2.5. Consequently, as the bandwidth was reduced the center frequency was shifted to lower frequency. The effects of the shift in center frequency due to attenuation on the REC technique will be discussed in Section 2.2.1.

2.1.4 Conclusion

The results of this study indicate that unless the harmonics are filtered prior to compression, the use of a Wiener filter operating as an inverse filter should be avoided in order to obtain adequate compression performance that minimizes sidelobe levels. The tradeoffs in moving away from an inverse filter are that the improvements in the axial resolution are minimized and sidelobes can be increased. When the echo signals were filtered prior to compression, significant improvements in both sidelobe levels and axial resolution were achieved by forcing the Wiener filter closer to an inverse filter state. Finally, attenuation could be a significant contributor in removing some of the distortion effects caused by nonlinear propagation, which would allow for improved compression performance.

2.2 Practical Limitations of the REC Technique

During the course of this study there were several limitations or hypothetical limitations encountered and characterized involving the REC technique. These limitations will be highlighted in the subsequent sections.

2.2.1 Center frequency shift and bandwidth reduction due to attenuation

The effects of frequency-dependent attenuation on coded signals have been investigated by several researchers [5, 10]. Therefore, the most significant effect that needed to be quantified in terms of the REC technique was the shift in center frequency caused by frequency-dependent attenuation and the amount of bandwidth reduction. It was hypothesized that the bandwidth using REC would have a larger shift in center frequency due to frequency-dependent attenuation as it contains a larger bandwidth compared to CP methods. The shift in center frequency can be modeled by describing the impulse response as a Gaussian function defined by

$$H(f) = Ae^{-\frac{(f-f_0)^2}{2\sigma^2}}, \tag{2.19}$$

where f is the frequency, A is the amplitude of the bandwidth at the center frequency, f_0, and σ is the standard deviation of the Gaussian distribution which would be representative of the bandwidth. The effects of frequency-dependent attenuation can be determined by multiplying the impulse response by the attenuation term assuming the attenuation coefficient is linear with frequency,

$$H(f,x) = Ae^{-\frac{(f-f_0)^2}{2\sigma^2}} \times e^{-4\alpha_0 fx}, \tag{2.20}$$

where α_0 is the attenuation coefficient (Np MHz^{-1} cm^{-1}) and x is the propagated distance into the media (in cm). After simplification the modified impulse response is given by

$$H(f,x) = Ae^{-\frac{(f^2-2ff_0+f_0^2-4\alpha_0 fx2\sigma^2)}{2\sigma^2}}. \tag{2.21}$$

To obtain the new center frequency, the maximum peak value was found by taking

the derivative of the expression in (2.21) and equating to zero,

$$\frac{d}{df}\left\{\frac{f^2 - 2ff_0 + f_0^2 - 4\alpha_0 f x 2\sigma^2}{2\sigma^2}\right\} = 0 \tag{2.22}$$

$$\frac{-f - 4\alpha_0 x\sigma^2 - f_0}{\sigma^2} = 0. \tag{2.23}$$

Solving for f, which is the new center frequency, the following is obtained:

$$f = f_0 - 4\alpha_0 x\sigma^2. \tag{2.24}$$

The expression in (2.24) indicates that by using the REC technique the center frequency will shift by a larger amount than CP because REC has a larger bandwidth. This phenomenon was further investigated by evaluating the effects of frequency-dependent attenuation in an experimental setting. The pre-filtered uncompressed echo data from the nonlinear propagation study was modified by multiplying with a frequency-dependent attenuation term to simulate the effects of tissue attenuation synthetically on experimental data. Based on the attenuation coefficient values listed in Table 2.2, attenuation coefficients of 0.0, 0.1, 0.3, 0.5, and 1.0 dB $\text{MHz}^{-1}\text{cm}^{-1}$ were evaluated. The experimental findings regarding center frequency shift for CP and REC (both a Wiener filter approaching an inverse filter (IF) and a Wiener filter approaching a matched filter (MF)) are summarized in Table 2.4. The bandwidth for CP was slightly less than REC-MF which was less than the bandwidth of REC-IF. The relative center frequency shift is shown in Fig. 2.6. Examination of Fig. 2.6 indicates that the smallest center frequency shift occurred with REC-MF. REC-MF obtained a small shift in center frequency because of the tremendous amount of bandwidth loss that resulted from the mismatch between the transmitted and received signals upon compression. Furthermore, as expected, the largest center frequency shift was obtained for REC-IF. This larger center frequency shift was a result of having the largest bandwidth.

Decreases in bandwidth due to attenuation were also observed (see Table 2.5 and Fig. 2.7). Interestingly, it was observed that the CP bandwidth increased for some attenuation values and then decreased for as the attenuation values got larger. This phenomenon occurred because the actual shape of the spectrum was asymmetrical. This phenomenon is shown in Fig. 2.8. For the pulse from the transducer, a sharper

falloff was observed in the bandwidth after the center frequency then before the center frequency. Therefore, when multiplying by a decaying exponential (attenuation) the bandwidth became larger for some small attenuation values. With REC, this increase in center frequency was not present as the pre-enhanced chirp boosted the frequencies in a manner such that the resulting bandwidth would be more symmetrical. Figure 2.9 shows regression analysis performed on the bandwidth data from Fig. 2.7. The points in the CP data that corresponded to increased bandwidth were not used in the regression analysis. For $\alpha = 0.5$, the -6 dB bandwidths for CP, REC-IF, and REC-MF were the same. Furthermore, for $\alpha < 0.5$ REC-IF provided the best results because the -6 dB bandwidth was larger, which means improved resolution. For $\alpha > 0.5$, CP provided the best results in terms of the -6 dB bandwidth. Of course, attenuation is depth-dependent and for this particular scenario the measurements were performed at the focus. Therefore, as the object is moved closer to the source, the performance for REC-IF and REC-MF is enhanced when compared to CP. As the object moves farther away from the source, CP may perform better in terms of bandwidth. The energy in the higher frequencies in REC is still greater than for CP due to the pre-enhanced chirp used to excite the source. Therefore, with appropriate depth-dependent filtering, the enhanced bandwidth of REC may be partially restored.

2.2.2 Transducer heating due to coded excitation

When sources are excited with a coded signal, it is possible that the source can heat leading to the possibility of burning tissue or skin if the probe is placed against the skin. The use of a pre-enhanced chirp was hypothesized to lead to even more heating tha a conventional linear chirp because it was expected that the excitation of the inefficient bands of the transducer would transfer more energy to heat. The idea is that preferentially exciting the inefficient bands with more energy would increase the surface temperature of the transducer, which could be potentially harmful to the patient being imaged.

The standard which characterizes the procedure for thermal measurements of sources (IEC 60601-2-37) indicates that surface temperature measurements should be conducted in air. However, measurements performed in air cause a reflection of the acoustic power

because of the impedance mismatch, which causes self-heating. Therefore, these measurements are considered to be a worst-case scenario. The temperature at which damage to the skin starts to occur is 56 °C [29].

To evaluate the effects of heating, measurements were performed with a single-element transducer (f/3) having a center frequency of 3 MHz and a -6 dB bandwidth of 33%. A noncontact infrared thermometer (Fluke 61, Everitt, WA) with a nominal manufacturer specified resolution of 0.2 °C and an accuracy of ± 2 °C was used. The measurements were performed in air with the thermometer at 152.4 mm away from the transducer. At this distance, the infrared thermometer provided an effective spot size of 19.05 mm, which was equivalent to the diameter of the transducer. The experiment consisted of exciting the transducer at different frequencies using a continuous sinusoidal excitation at different voltage levels. Specifically, frequencies ranging from 1 MHz to 6 MHz in increments of 1 MHz and excitation voltages of 50 mV, 100 mV, and 200 mV out of the Tabor AWG were used. These voltages were amplified by a 50 dB power amplifier (ENI 2300L, Rochester, New York). The results of the measurements are shown in Fig. 2.10. The results provide sufficient evidence that heating mostly occured at the fundamental frequency of the transducer and not at the band edges.

A pre-enhanced chirp with pulse repetition frequencies of 0.5 kHz, 1 kHz, and 2 kHz and a various excitation voltages (50 mV, 100 mV, and 200 mV) were tested. For the 0.5 kHz, and 1 kHz pulse repetition frequencies, the measured temperatures were near room temperature (¡ 1% variation). The thermal measurements obtained when exciting with a pre-enhanced chirp for the 200 mV case are shown in Fig. 2.10. The results of this test did not support the hypothesis that exciting with more energy in the inefficient bands of the transducer would lead to more heating over conventional linear chirps. Therefore, a new hypothesis was proposed that exciting the transducer with a pre-enhanced chirp resulted in more energy at the inefficient bands to be reflected back to the power amplifier. This new hypothesis will have to be further tested in the future by using a KLM model (developed by Krimholtz, Leedom, and Matthaei [30]) to characterize the pressure versus voltage characteristics of a piezoelectric transducer with a pre-enhanced chirp excitation to predict heating in the source. However, the pre-enhanced chirp was not observed to produce significant heating beyond a linear

chirp excitation.

2.2.3 Pressure-limited vs. voltage-limited chirps and their effect on eSNR

The main goal of the pre-enhanced chirp is to pump more energy into the band edges in order to obtain a wider and flatter system response in terms of bandwidth. Consequently, less energy is applied at the frequencies near the center frequency compared to the band edges. In this scenario, the pre-enhanced chirp is considered to be voltage-limited when the maximum voltage that can be applied to the transducer corresponds to the maximum value of the pre-enhanced chirp. If the pre-enhanced chirp was compared to a linear chirp and if the peak voltage of both signals applied to the transducer were the same, then a drop in the pressure output would be observed for excitation using the pre-enhanced chirp. A drop in pressure could be viewed as an advantage in that there is less potential for bioeffects or for nonlinear distortion. However, the disadvantage is that the eSNR would be smaller because less energy is contained in the pre-enhanced chirp compared to the linear chirp.

The drop in eSNR was evaluated by generating several pre-enhanced chirps in MATLAB for various sources with different fractional bandwidths. The results of this study are shown in Fig. 2.11. Examination of Fig. 2.11 suggests that the lower the original bandwidth of the source and the more axial resolution boost from REC, the smaller the eSNR. Therefore, in the voltage-limited case a tradeoff between the eSNR and the amount of axial resolution boost achievable with REC was observed. Most sources used in this REC study had a fractional bandwidth on the order of 75%. If the bandwith was doubled to 150%, according to Fig. 2.11, a 7 dB drop in eSNR would be obtained when compared to a linear chirp excitation. This lower eSNR comes from the fact that the amplitude of the pre-enhanced chirp at the center frequency is lower than the amplitude of the pre-enhanced chirp at the band edges. However, a linear chirp excitation would have a higher pressure output level, which could introduce bioeffects and increase the possiblity of nonlinear effects, and would not have the benefits of a larger bandwidth provided by REC.

Although a decrease in eSNR when exciting with a pre-enhanced chirp is dependent on source bandwidth and pre-enhanced chirp boost, a gain in eSNR is obtained after

compression by a factor related to the TBP. Therefore, consideration must be taken in the design of the code in terms of desired boost and code length (i.e., the larger the code the longer the dead zone in the image). For example, assume that an ultrasound system that was excited with a linear chirp (TBP = 40) resulted in an eSNR of 50 dB prior to compression when using a 10 MHz (75% bandwidth) transducer. If the source bandwidth was doubled to 150% using a pre-enhanced chirp with a TBP of 40, a reduction of 7 dB in eSNR would be obtained according to Fig. 2.11. Therefore, the resulting eSNR prior to compression would be 43 dB. In coded excitation schemes, the eSNR increases upon compression by a factor related to the TBP. Because the TBP was the same for the linear chirp and the pre-enhanced chirp, the eSNR was effectively smaller for REC when compared to the linear chirp, but higher than the precompressed output eSNR. Moreover, because the bandwidth in REC was larger and TBP for the linear chirp and the pre-enhanced chirp were the same, the time duration of the pre-enhanced chirp was smaller, resulting in a smaller dead zone. Finally, the increase in bandwidth resulted in an improved image because of the improved axial resolution.

The case when the maximum pressure output was the same for both codes was also studied. This case is contrasted with the previous case where the voltage input was the limiting value. In this scenario, the linear chirp was considered to be pressure-limited in that the input voltage to the transducer was not the limiting factor but the subsequent output pressure was the limiting factor. Because the intensity levels of diagnostic ultrasound are regulated by the FDA, as long as the transducer can handle high voltages, the only limitation may be the output pressure from the excitation levels, i.e., a transducer is more likely to be pressure-limited vs. voltage-limited in a clinical system. When a pressure-limited linear chirp was compared to a pre-enhanced chirp it was observed that the eSNR was slightly higher for REC because both chirps had equal energy at the center frequency but the pre-enhanced chirp boosted the energy in the band edges. Consequently, the transducer was being excited with more energy using pre-enhanced chirp. The drawback for the linear chirp was that, because the voltage was reduced, the eSNR was reduced. The results of this study lead to the conclusion that as long as the output intensity is within regulations, driving the transducers at the highest possible voltages yield the best performance. The driving voltages would

need to be optimized for individual transducers taking into account the durability of the transducers to higher voltages at the inefficient bands.

The main limitation in experimental scheme was that the power amplifiers used to provide the high voltage signals in to the transducers resulted in a voltage-limited scenario. These amplifiers had an input voltage limitation of $1V_{RMS}$. Therefore, if a pre-enhanced chirp had a peak value at $1V_{RMS}$, the voltage at the center frequency would be at best $0.5V_{RMS}$ if the bandwidth was only doubled. The implications were that the maximum linear chirp voltage would be $0.5V_{RMS}$, which means that the voltage of the linear chirp was being limited by the power amplifier. As a result, the linear chirp was voltage-limited in that improved results could be achieved with a voltage higher than $0.5V_{RMS}$.

Another item of importance is the maximum voltage that can be applied to transducers. Transducers have a voltage limit that is dictated by the Curie temperature of the crystal. If a transducer reaches the Curie temperature, then the transducer's crystal depolarizes which makes the transducer useless. Therefore, special care must be taken so that the voltage input does not exceed this limit at the band edges. For a transducer with a lithium niobate crystal the Curie temperature is 1415 ° C [31].

2.3 Conclusions

In the previous sections, the REC technique was characterized and practical limitations were discussed. The detrimental effects of nonlinear distortion on the compression of REC echoes were evaluated. Overall, amplification of the harmonics when the Wiener filter operated near inverse filter mode affected the compression performance the most compared to a matched filter. When the harmonics were amplified the sidelobe levels being produced were significantly higher than when no harmonics were present. Consequently, the compression performance was improved by pre-filtering the higher harmonics to reduce sidelobe levels.

The effects of frequency-dependent attenuation and pre-enhanced chirp construction limitations were examined. Specifically, the effects that attenuation had on REC because of its larger bandwidth were examined. Overall, attenuation caused a larger center frequency shift and resulted in a larger bandwidth loss with REC than with CP.

Furthermore, the pre-enhanced chirp was evaluated in terms of center frequency amplitude versus peak amplitude. It was concluded that pressure-limited case should results in the best performance of REC in terms of eSNR and compression. However, by exciting the transducers with higher voltages, the crystal stability could be compromised and the lifetime of the transducer could be reduced.

Finally, the possible heating of the source when excited with a pre-enhanced chirp was evaluated. The pre-enhanced chirp did not produce any significant source heating greater than would be achieved with a similar linear chirp. Therefore, it was concluded that heating of the source was not of greater concern using the REC method.

Overall, the engineering tradeoffs encountered during the practical limitation studies were: nonlinear distortion vs. sidelobes, bandwidth boost vs. eSNR, attenuation vs. center frequency shift, and attenuation vs. bandwidth.

2.4 Figures and Tables

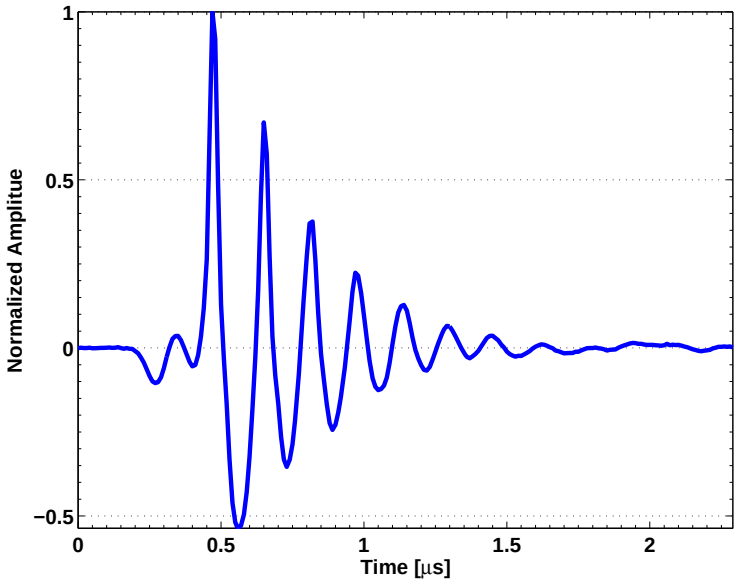

(a)

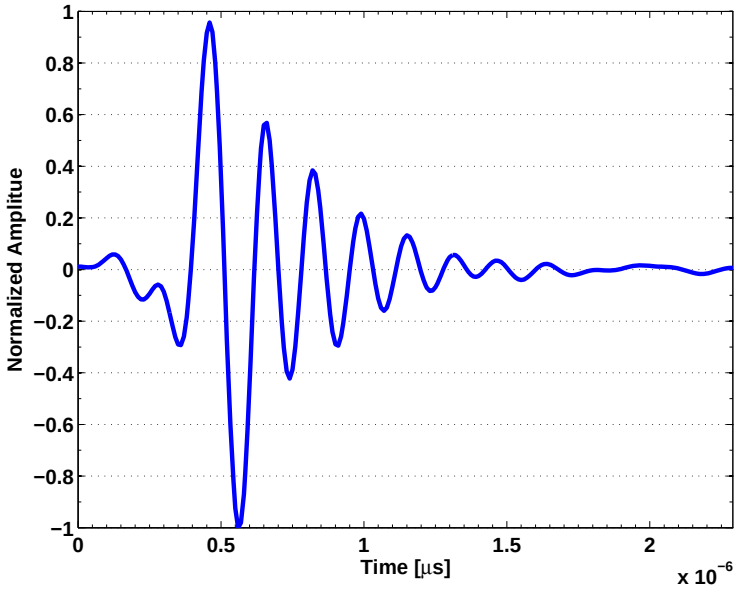

(b)

Figure 2.1: An ultrasonic waveform (a) exhibiting and (b) not exhibiting the effects of nonlinear distortion.

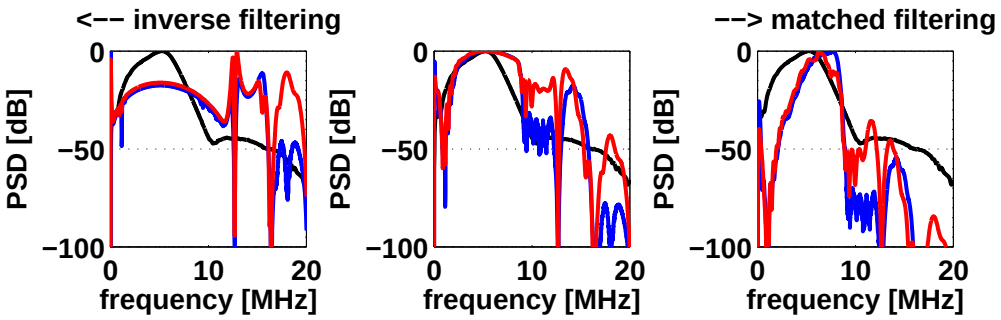

(a)

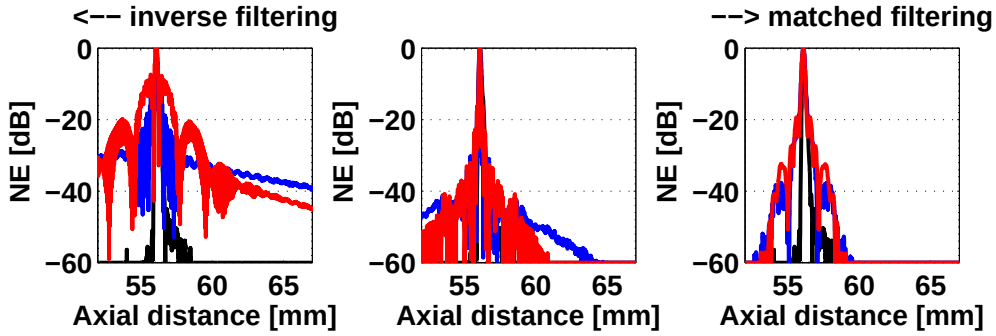

(b)

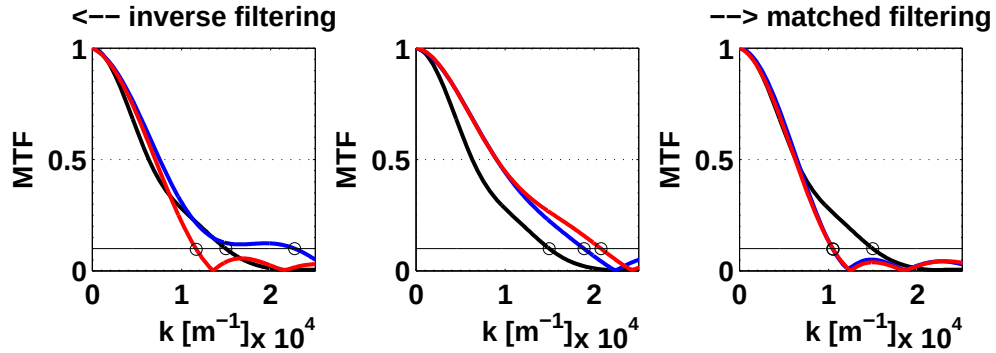

(c)

Figure 2.2: (a) PSD as a function of frequency, (b) normalized envelope as a function of axial distance, and (c) MTF as a function of wave number. From left to right shows the effects of changing the Wiener filter gamma parameter. CP is shown in black while REC values are shown in blue (1.3 MPa), and red (4 MPa). Note that the CP result is only shown as a reference and does not undergo distortion due to nonlinear propagation.

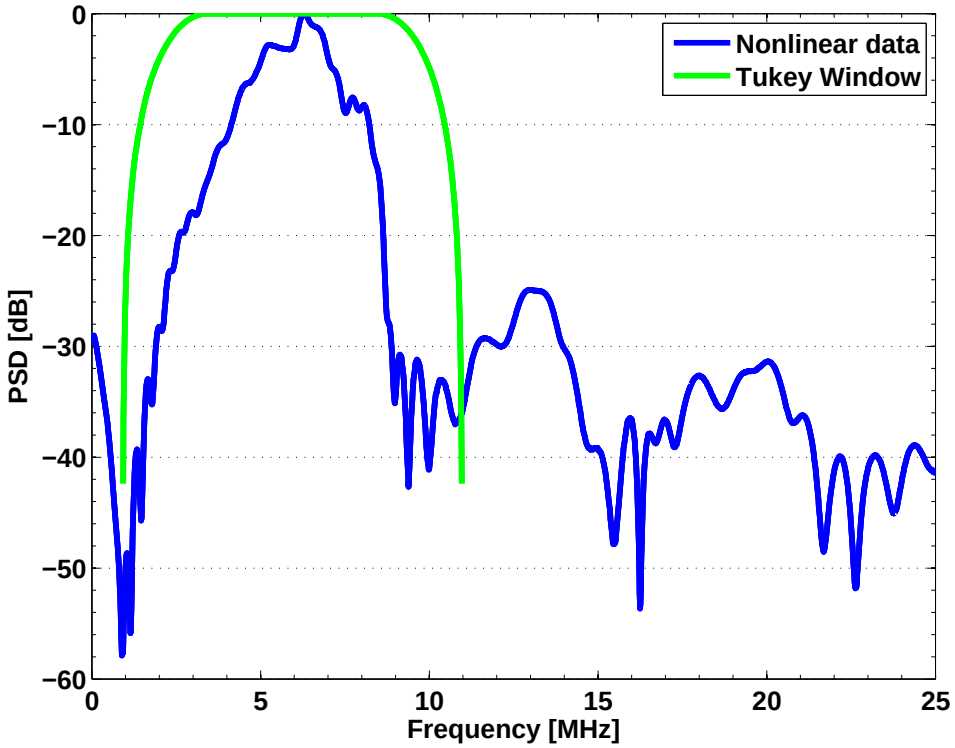

Figure 2.3: Application of a Tukey window on a pre-compressed echo to remove the higher harmonics caused by nonlinear propagation.

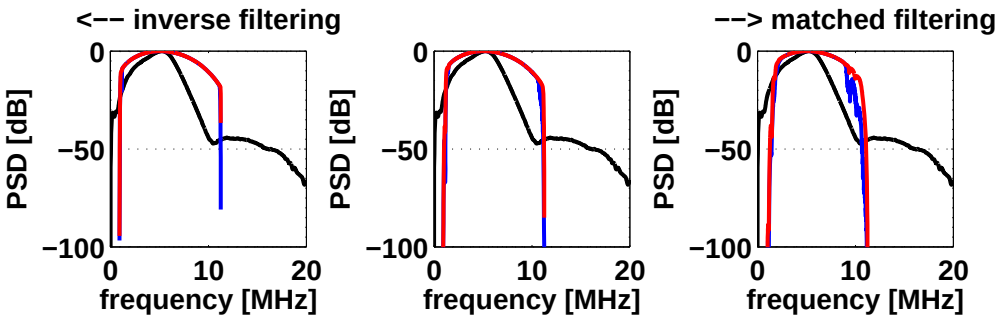

(a)

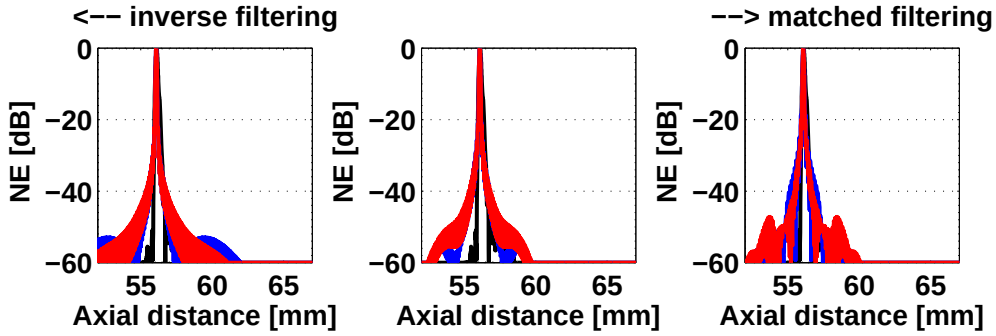

(b)

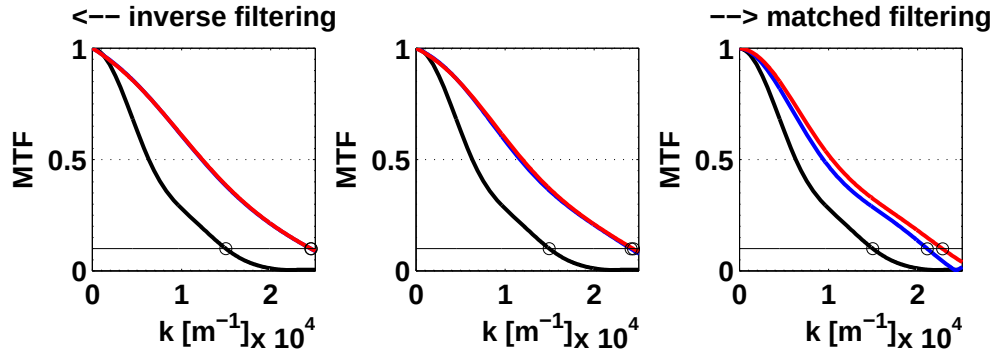

(c)

Figure 2.4: (a) PSD as a function of frequency, (b) normalized envelope as a function of axial distance, and (c) MTF as a function of wave number for the case that includes a post-filter to remove harmonics introduced due to distortion. From left to right shows the effects of changing the Wiener filter gamma parameter. CP is shown in black while REC values are shown in blue (1.3 MPa), and red (4 MPa). Note CP result is only shown as a reference and does not undergo distortion due to nonlinear propagation.

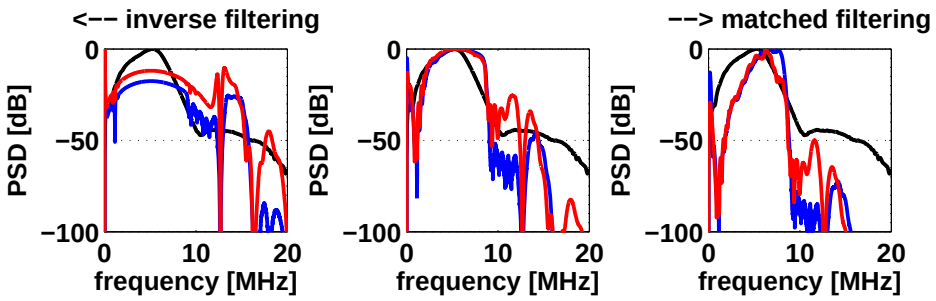

(a)

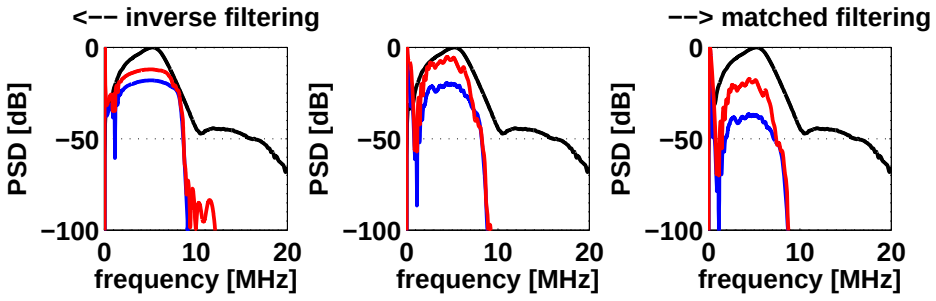

(b)

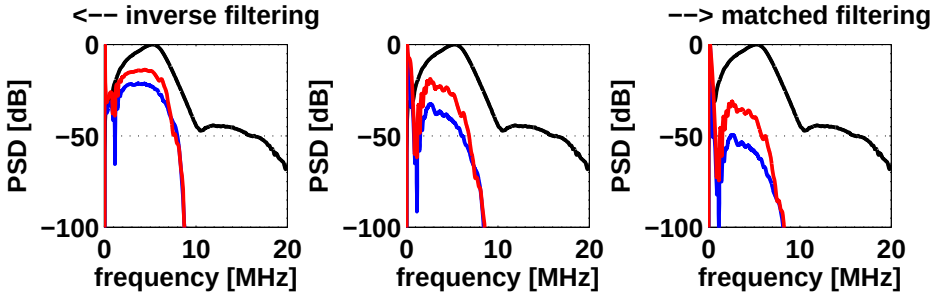

(c)

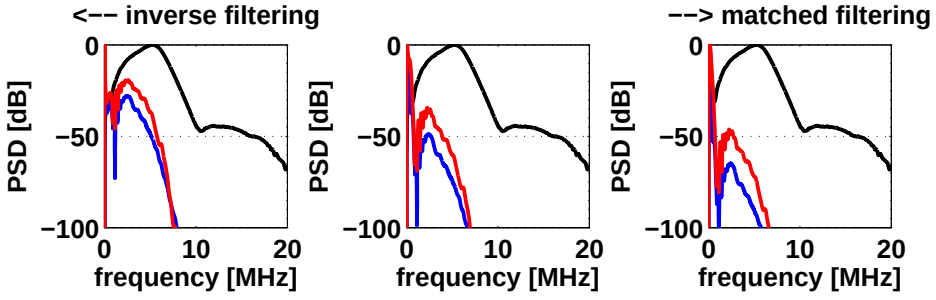

(d)

Figure 2.5: PSD as a function of frequency for different attenuation coefficients: (a) 0.1, (b) 0.5, (c) 0.7 and (d) 1.0 dB $\mathrm{MHz}^{-1}\mathrm{cm}^{-1}$.

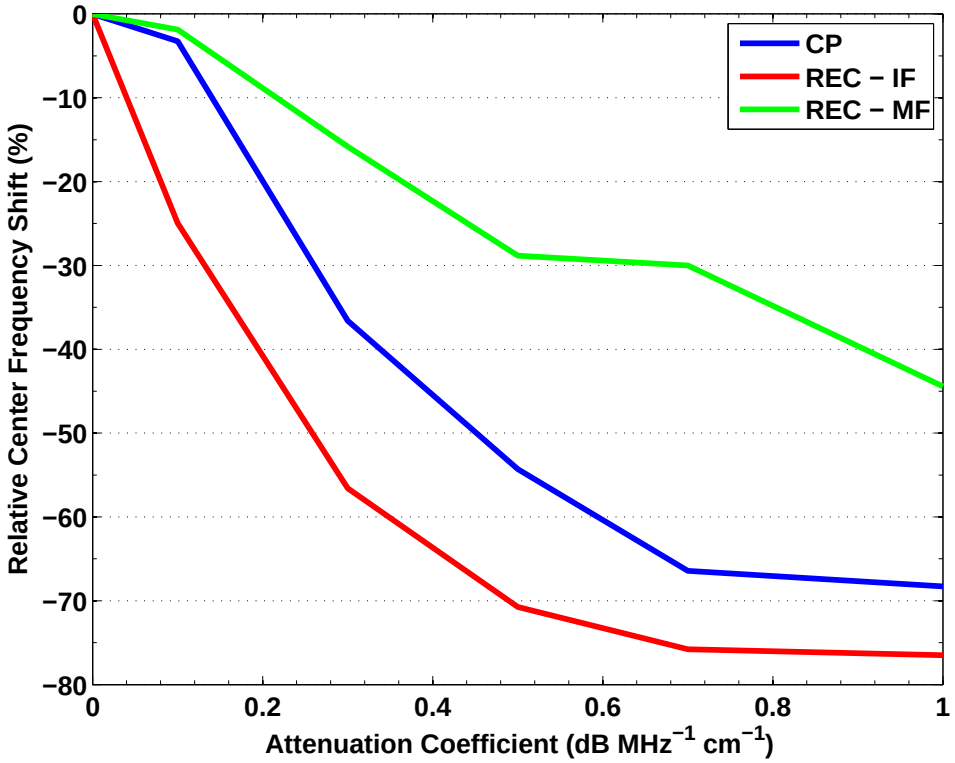

Figure 2.6: Relative frequency shift as a function of attenuation coefficient for CP and REC. REC was evaluated under two compression scenarios: a Wiener filter approaching an inverse filter (REC-IF) and a Wiener filter approaching a matched filter (REC-MF).

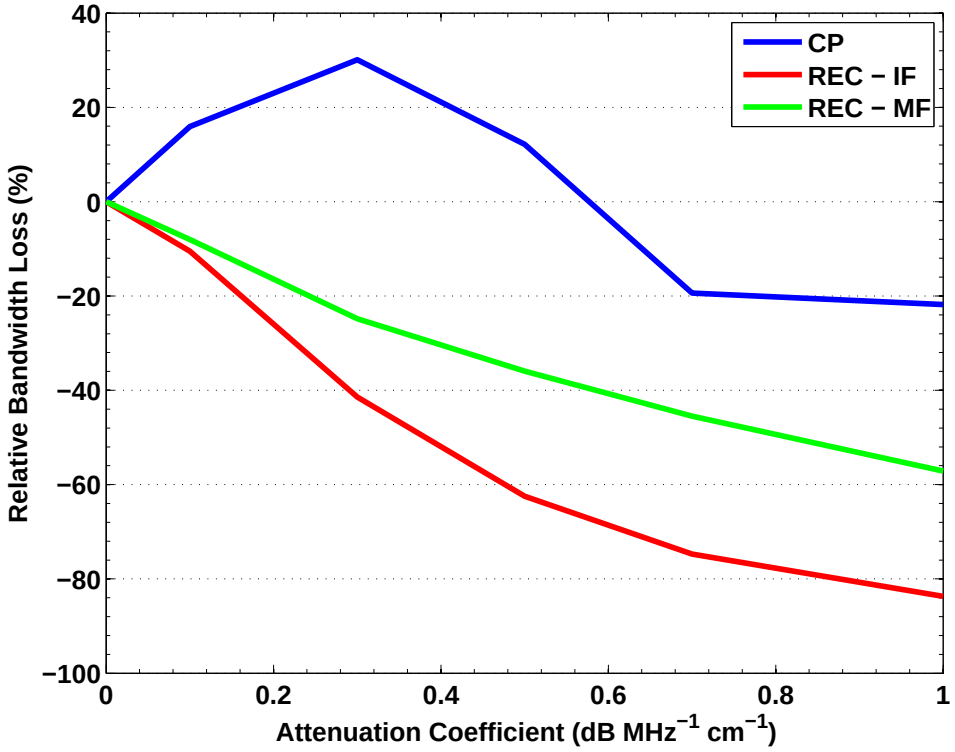

Figure 2.7: Relative bandwidth loss as a function of attenuation coefficient for CP and REC. REC was evaluated under two compression scenarios: a Wiener filter approaching an inverse filter (REC-IF) and a Wiener filter approaching a matched filter (REC-MF).

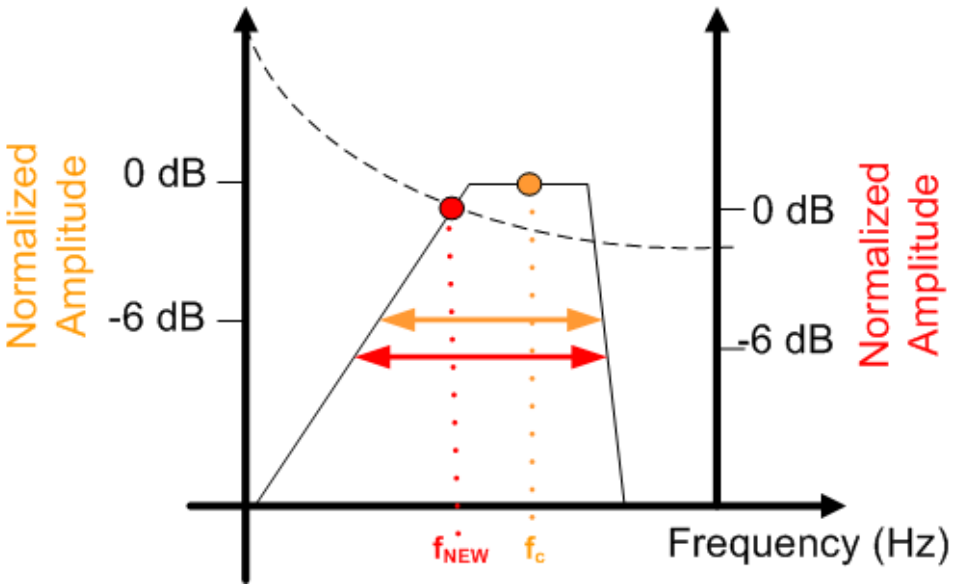

Figure 2.8: Example showing how a nonsymmetrical system function can become larger by an attenuating function. Items in orange show the original system function with the smaller bandwidth and the items in red show the system function with the larger bandwidth. Note that the ordinate is normalized amplitude and that in the scenario where the system function was attenuated the scale shifts due to normalization. f_c represents the center frequency while f_{NEW} represent the shift in center frequency.

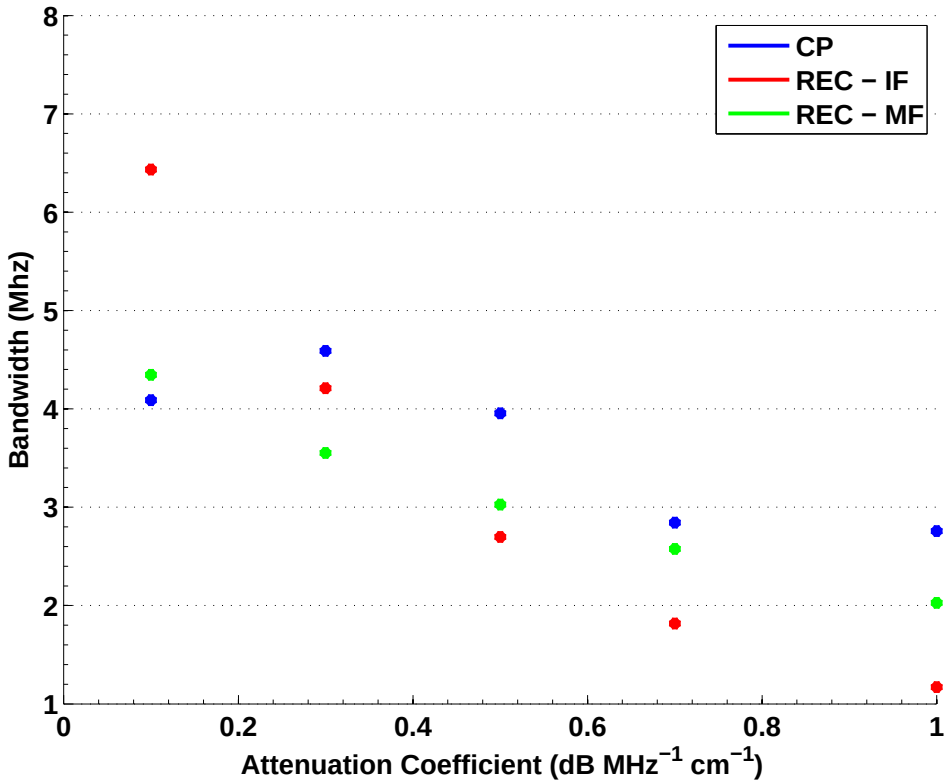

Figure 2.9: Bandwidth as a function of attenuation coefficient for CP and REC. REC was evaluated under two compression scenarios: a Wiener filter approaching an inverse filter (REC-IF) an a Wiener filter approaching a matched filter (REC-MF).

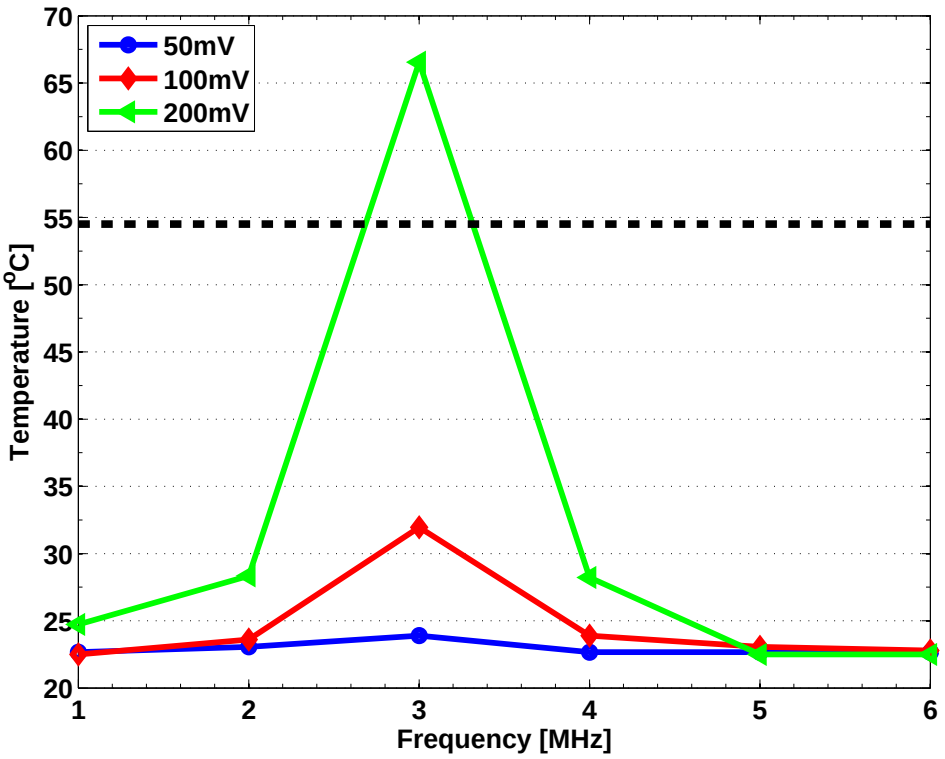

Figure 2.10: Thermal measurements of a 3 MHz transducer as a function of frequency for a continuous sinusoid excitation. Dashed line indicates the temperature at which skin starts to burn.

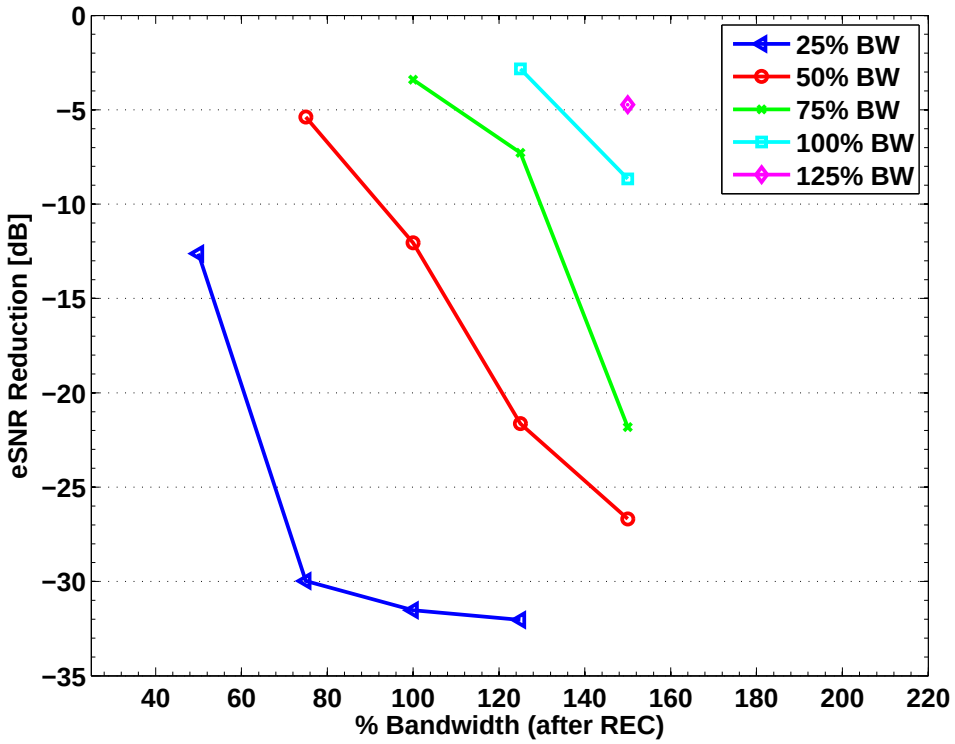

Figure 2.11: Reduction of eSNR as a function of the fractional bandwidth. The legend represents the original transducer bandwidth while the x-axis represents the bandwidth value achieved using REC. These results were obtained for a TBP of 40.

Table 2.1: A summary of SHFR, SMR (long-range (LR) and short-range (SR)), and MTF for the nonlinear effects study. The operating point of the Wiener filter was adjusted to obtain an inverse filter (IF), a matched filter (MF) and a middle approach between these extremes (MA).

Parameter	Pressure	IF	MA	MF
SHFR	1.3 MPa	0 dB	-31 dB	-70 dB
	4.0 MPa	0 dB	-17 dB	-36 dB
SMR-LR	1.3 MPa	-30 dB	-30 dB	-37 dB
	4.0 MPa	-20 dB	-34 dB	-32 dB
SMR-SR	1.3 MPa	-14 dB	-30 dB	-25 dB
	4.0 MPa	-10 dB	-32 dB	-20 dB
MTF	1.3 MPa	138 μm	166 μm	300 μm
	4.0 MPa	269 μm	151 μm	298 μm

Table 2.2: Attenuation coefficients of some common human soft tissues.

Tissue Type	α_{dB} (dB MHz^{-1}cm^{-1})
Blood	0.20
Breast	0.75
Fat	0.48
Kidney	1.0
Liver	0.5
Muscle	1.09
Skin	0.35

Table 2.3: SHFR results when applying attenuation to the distorted signals due to nonlinear propagation at the focal depth (55 mm) of a 5 MHz (f/3) source.

Attenuation Coefficient	Inverse Filter		Matched Filter	
	1.3 MPa	4 MPa	1.3 MPa	4 MPa
(dB $MHz^{-1}cm^{-1}$)	(unitless)	(unitless)	(unitless)	(unitless)
0.0	-0	-0	-70	-36
0.1	-0	-8	-72	-50
0.3	-26	-50	$\leq$-100	-75
0.5	$\leq$-100	-71	$\leq$-100	$\leq$-100
1.0	$\leq$-100	$\leq$-100	$\leq$-100	$\leq$-100

Table 2.4: Center frequency shift after synthetically adding attenuation to the pre-compressed echoes. CP center frequency shift shown as reference.

Attenuation Coefficient	CP	REC	
		Inverse Filter	Matched Filter
(dB $MHz^{-1}cm^{-1}$)	(MHz)	(MHz)	(MHz)
0.0	0.00	0.00	0.00
0.1	-0.17	-1.27	-0.10
0.3	-1.91	-2.88	-0.83
0.5	-2.84	-3.60	-1.51
0.7	-3.47	-3.85	-1.58
1.0	-3.57	-3.89	-2.33

Table 2.5: Bandwidth after synthetically adding attenuation to the pre-compressed echoes. CP bandwidths shown as reference.

Attenuation Coefficient (dB $MHz^{-1}cm^{-1}$)	CP (MHz)	REC	
		Inverse Filter (MHz)	Matched Filter (MHz)
0.0	3.52	7.19	4.72
0.1	4.09	6.43	4.34
0.3	4.59	4.21	3.55
0.5	3.96	2.70	3.02
0.7	2.84	1.81	2.57
1.0	2.75	1.17	2.02